DALTON
FULL PAPER

Migration of a phenyl group from co-ordinated $CH_2(PPh_2)_2$ to an acetylide on an Ru_3 cluster: crystal structure of $[Ru_3(\mu\text{-}H)(\mu_3\text{-}PPhCH_2PPh_2)(\mu_3\text{-}PhC_2Bu^t)(CO)_6]$†

Michael I. Bruce,*[a] Paul A. Humphrey,[a] Brian W. Skelton,[b] Allan H. White,[b] Karine Costuas[c] and Jean-François Halet[c]

[a] *Department of Chemistry, University of Adelaide, Adelaide, South Australia 5005, Australia. E-mail: mbruce@chemistry.adelaide.edu.au*
[b] *Department of Chemistry, University of Western Australia, Nedlands, Western Australia 6907, Australia*
[c] *Laboratoire de Chimie du Solide et Inorganique Moléculaire, UMR CNRS 6511, Université de Rennes 1, 35042 Rennes Cedex, France*

Received 8th September 1998, Accepted 18th November 1998

Thermolysis (refluxing toluene, 60 h) of $[Ru_3(\mu\text{-}H)(\mu_3\text{-}C_2Bu^t)(\mu\text{-}dppm)(CO)_7]$ resulted in phenyl transfer from co-ordinated dppm to the μ_3-acetylide to give $[Ru_3(\mu\text{-}H)(\mu_3\text{-}PPhCH_2PPh_2)(\mu_3\text{-}PhC_2Bu^t)(CO)_6]$ in 41% yield, fully characterised by X-ray determinations of thf and CH_2Cl_2 monosolvates. The alkyne is co-ordinated to the Ru_3 cluster such that the C(1)–C(2) vector forms an angle of 23° with the Ru(1)–Ru(2) vector. This distortion brings two C atoms of the alkyne Ph group close to Ru(2). Density functional and extended Hückel calculations carried out on the new compound indicated that the unusual co-ordination of the alkyne ligand can be attributed to the stereoelectronic asymmetry of the metallic fragment.

Introduction

The chemistry of $[Ru_3(\mu\text{-}dppm)(CO)_{10}]$ **1** (Scheme 1) has been well developed in recent years.[1] One of its characteristic reactions is the ready loss of a phenyl group by cleavage of a P–C bond. Thus, hydrogenation of **1** afforded $[Ru_3(\mu\text{-}H)(\mu_3\text{-}PPhCH_2PPh_2)(CO)_9]$ **2**, probably *via* an intermediate cluster hydride, the phenyl group combining with one H atom to give benzene.[2] This process was observed directly during the pyrolysis of $[Ru_4(\mu\text{-}H)_4(\mu\text{-}dppm)(CO)_{10}]$, which afforded $[Ru_4(\mu\text{-}H)_3(\mu_3\text{-}PPhCH_2PPh_2)(CO)_9]$.[3] An alternative source of the hydrogen atom is a phenyl group on the second P atom, which becomes metallated in the complex $[Ru_3\{\mu_3\text{-}PPhCH_2PPh(C_6H_4)\}(CO)_9]$ **3**.[2] It is likely that *ortho*-metallation of this phenyl group occurs prior to elimination of benzene, as found for several aryl-phosphine cluster complexes.[4] An alternative product, formed under CO, is **4**, which contains the unusual chelating bridged ditertiary phosphine $C_6H_4(PPhCH_2PPh)$.[2]

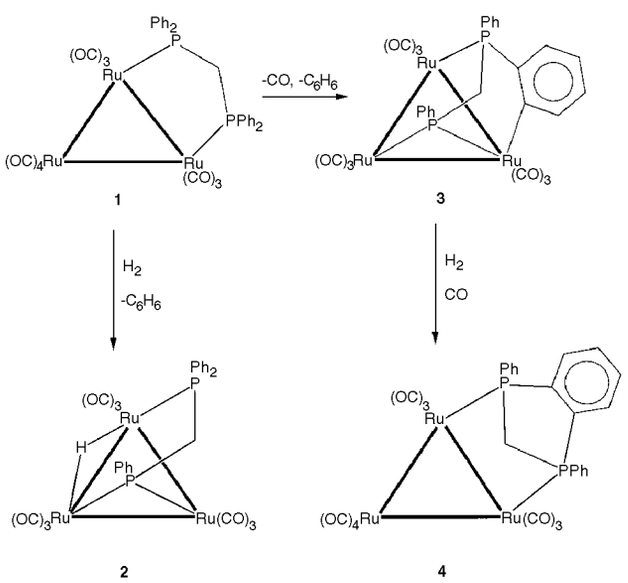

1 **3** **2** **4**

Scheme 1

In all of these reactions the phenyl group has been eliminated from the precursor complex, no phenylated derivatives having been isolated. We have recently described the formation of the cluster phenyl complexes $[Ru_3(\mu_3\text{-}PPhCH_2PPh_2)(\mu_3\text{-}C_8H_8)(Ph)(CO)_5]$[5] and $[Ru_3(\mu_3\text{-}PPhCH_2PPh_2)(\mu_3\text{-}C_2PPh_2)(\mu\text{-}PPh_2)(Ph)(CO)_6]$,[6] in both of which the Ph group is trapped on the cluster. In the course of studies of the reactions of **1** with various alkynes,[7] we have found an example of migration of a phenyl group to a cluster-bound alkynyl group to give an alkyne which is attached to the cluster in an unusual way.

Results

We have described elsewhere[5] the ready addition of terminal alkynes to **1** to give the complexes $[Ru_3(\mu\text{-}H)(\mu_3\text{-}C_2R)(\mu\text{-}dppm)(CO)_7]$ **5** (Scheme 2). On heating the *tert*-butyl complex **5** (R = Bu^t) in refluxing toluene for an extended period a new red complex was isolated in 41% yield and identified as $[Ru_3(\mu\text{-}H)(\mu_3\text{-}PPhCH_2PPh_2)(\mu_3\text{-}PhC_2Bu^t)(CO)_6]$ **6** by a single-crystal X-ray determination.

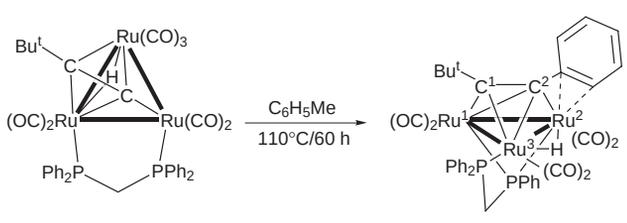

5 **6**

Scheme 2

† Dedicated to Warren Roper on the occasion of his 60th birthday, in recognition of his outstanding contributions to organometallic chemistry.

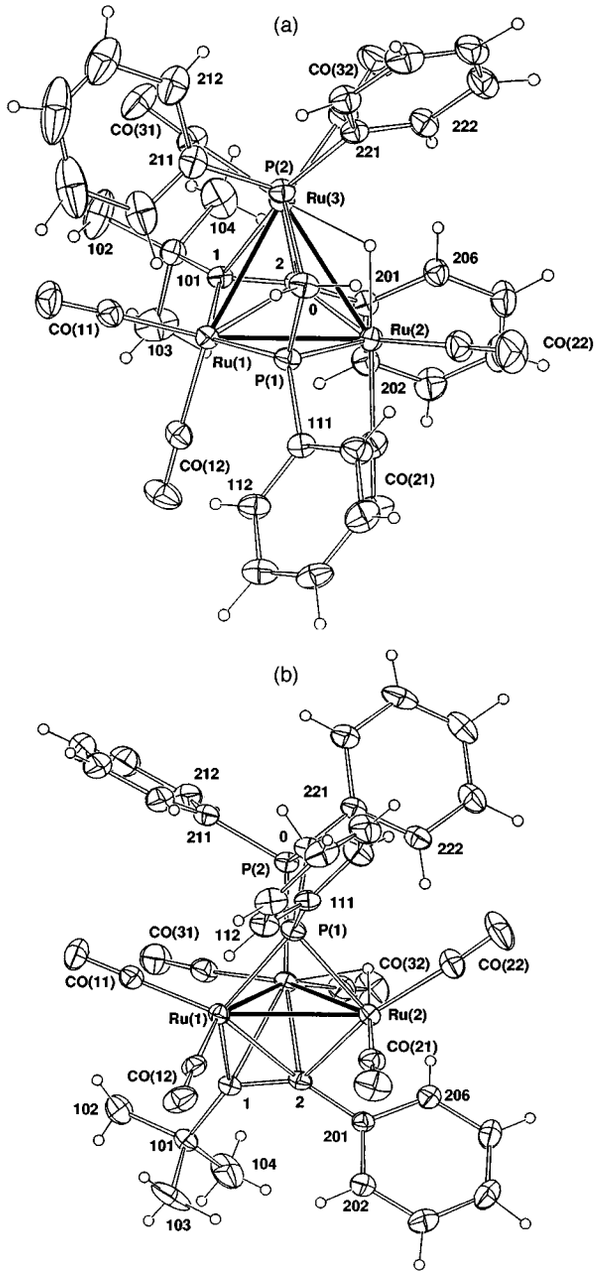

Fig. 1 Projections of $[Ru_3(\mu\text{-H})(\mu_3\text{-PPhCH}_2\text{PPh}_2)(\mu_3\text{-PhC}_2\text{Bu}^t)(CO)_6]$ **6** (thf solvate), (a) normal to and (b) 'through' the Ru_3 plane; 20% thermal ellipsoids are shown for the non-hydrogen atoms, hydrogen atoms having arbitrary radii of 0.1 Å.

Crystal and molecular structures of $[Ru_3(\mu\text{-H})(\mu_3\text{-PPhCH}_2\text{PPh}_2)(\mu_3\text{-PhC}_2\text{Bu}^t)(CO)_6]$ 6

As described at length below, crystals of compound **6** (Fig. 1) were obtained monosolvated with thf and CH_2Cl_2, a study of a less completely solvated form of the latter also being recorded. All forms crystallize in the orthorhombic space group *Pbca*; unit cell projections are given for the fully solvated thf monosolvate and the fractional [0.366(3)] dichloromethane solvate, projected down *a* and *b* in Fig. 2, cell volumes of these two extreme forms differing by more than 10%. Nevertheless, as the projections down *b* show, the *x* and *z* coordinates of the two forms are very similar, and it is also seen that the molecules may be considered to be disposed as layers about $c = 1/8, 3/8, 5/8, 7/8$. The relative alignments of successive layers change with respect to each other in *y*, however, and, in fact, the *y* coordinates of the defining molecule of the asymmetric unit are displaced between the two types of solvate by *ca*. a quarter of a cell in that dimension. Consideration has been given as to whether this change impacts on the structure of **6**; comparative geometries are given for the different forms in Tables 1 and 2, no non-trivial difference being observed in the associated bond lengths and angles. In terms of broader conformation, however, Table 2 shows the parameter most affected to be the pitch of the 22n ring plane *vis-à-vis* the rest of the molecule. Discussion of the individual molecule of **6** is now conducted in terms of the most precisely determined example in the thf solvate.

The complex contains a triangular cluster of three ruthenium atoms [Ru–Ru 2.7311(4)–2.8936(4) Å], each of which bears two CO groups. One face of the triangle is capped by a dephenylated dppm ligand, similar to those found in the other related complexes mentioned above. The Ru(1)–Ru(2) vector is bridged by the phosphido P atom [Ru(1,2)–P(1) 2.2901(8), 2.3254(8) Å] while P(2) is attached to Ru(3) [2.3235(8) Å], while the longer Ru(2)–Ru(3) vector is bridged by the hydride ligand [Ru(2,3)–H(23) 1.71(2), 1.80(2) Å].

The other face is capped by a PhC_2Bu^t ligand in a μ_3-η^2 mode with further interaction between C(201) and C(206) of the phenyl ring and Ru(2). The arrangement is shown in Figs. 1 and 3. The alkyne deviates somewhat from the symmetrical μ_3-η^2-(⊥) mode[8] [the projected angle between the Ru(1)–Ru(3) and C(1)–C(2) bonds is 23°]. This is reflected in the bond lengths Ru(1)–C(1) [2.035(3) Å] and Ru(1)–C(2) [2.426(3) Å] which are rather different from Ru(3)–C(1) [2.433(3) Å] and Ru(3)–C(2) [2.162(3) Å], respectively. Such a twist is accompanied by quite a large C(1)–C(2)–C(201) angle [142.1(3)°] and some C(101)–C(1)–C(2)–C(201) torsion [−34.8(6)°] which brings two carbon atoms of the Ph group, C(201) and C(206), close to Ru(2) [2.404(3) and 2.557(3) Å, respectively]. A rather strong interaction between Ru(2) and C(2) [2.273(3) Å] is also observed. The C(1)–C(2) bond length is 1.355(4) Å. We note also that there is some degree of localization of π-electron density in the intraring C–C bonds such that two [C(202)–C(203) 1.366(4), C(204)–C(205) 1.348(5) Å] are shorter than the other four [all greater than 1.388(5) Å], suggesting interaction of the ring π-electron density in C(201)–C(206) with Ru(2). The C(2)–C(201) separation is 1.455(4) Å. These tendencies are reproduced in the geometries of the CH_2Cl_2 solvate, albeit at a lower level of precision.

The spectroscopic properties of compound **6** are consistent with the solid-state structure. The solution IR spectrum contains six terminal ν(CO) bands while the ^{1}H NMR spectrum contains a complex multiplet at δ −17.56 which is assigned to the Ru–H proton. The CH_2 protons of the phosphorus ligand resonate between δ 4.0 and 4.5. A doublet at δ 5.69 can be assigned to a proton adjacent to the Ru-bonded phenyl carbon. The FAB mass spectrum contains M^+ centred around *m*/*z* 939, which decomposes by loss of H, CO, $PPhCH_2PPh_2$ and alkyne fragments.

The electron count for this cluster is interesting. A count of 46 "metallic" valence electrons (MVEs) is achieved assuming that the alkyne ligand donates four electrons to the cluster [24 (3 × Ru) + 1 (H) + 5 ($PPhCH_2PPh_2$) + 12 (6 × CO) + 4 (PhC_2Bu^t) = 46]. Such a count precludes any electron donation from the phenyl group attached to C(2) to the metallic array. The Polyhedral Skeletal Electron Pair (PSEP) theory supported by molecular orbital calculations has proven to be very helpful for understanding the structural chemistry of trimetallic alkyne cluster complexes.[9] Such compounds are mainly encountered in two distinct geometries depending on their electron counts. Species characterized by 46 MVEs adopt a *closo*-trigonal-bipyramidal structure with the alkyne moiety lying perpendicular to one metal–metal bond [μ_3-η^2-(⊥) mode],[8] such as $[Fe_3\{\mu_3\text{-}(\perp)\text{-}C_2Ph_2\}(CO)_9]$ **7**.[10] Those having 48 MVEs are generally found with a *nido*-square-pyramidal geometry with the acetylenic ligand positioned parallel to a metal–metal vector [μ_3-η^2-(‖) mode][8] as exemplified by $[Co_2Fe\{\mu_3\text{-}(\|)\text{-}C_2Et_2\}(CO)_9]$ **8**.[11] A third arrangement which can regarded as a skeletal isomer of the *nido* form, unexpected according to the PSEP

Table 1 Selected molecular geometries (distances in Å, angles in °) for $[Ru_3(\mu\text{-}H)(\mu_3\text{-}PPhCH_2PPh_2)(\mu_3\text{-}PhC_2Bu^t)(CO)_6]$ **6**. The three values in each entry are for **6**·thf, ·CH_2Cl_2 and ·0.366(3)CH_2Cl_2 respectively

Ru(1)–Ru(2)	2.8716(4), 2.866(2), 2.8701(6)	Ru(1)–Ru(2)–Ru(3)	56.551(8), 56.44(2), 56.45(1)
Ru(1)–Ru(3)	2.7311(4), 2.721(1), 2.7253(5)	Ru(2)–Ru(3)–Ru(1)	61.32(1), 61.35(4), 61.36(1)
Ru(2)–Ru(3)	2.8936(4), 2.889(1), 2.8928(6)	Ru(3)–Ru(1)–Ru(2)	62.132(9), 62.22(4), 62.20(1)
Ru(1)–P(1)	2.2901(8), 2.297(2), 2.293(1)	Ru(1)–P(1)–Ru(2)	76.94(3), 76.79(8), 77.05(3)
Ru(2)–P(1)	2.3254(8), 2.317(2), 2.315(2)	Ru(1)–P(1)–C(0)	120.6(1), 121.3(2), 120.8(1)
Ru(3)–P(2)	2.3235(8), 2.319(2), 2.327(1)	Ru(2)–P(1)–C(0)	108.4(1), 107.5(2), 107.9(1)
Ru(1)–C(1)	2.035(3), 2.040(7), 2.022(3)	Ru(3)–P(2)–C(0)	108.9(1), 107.8(2), 107.5(1)
Ru(1)–C(2)	2.426(3), 2.411(7), 2.412(3)	Ru(1)–C(1)–Ru(3)	74.78(8), 74.8(2), 74.8(1)
Ru(2)–C(2)	2.273(3), 2.258(6), 2.265(3)	Ru(2)–C(2)–Ru(3)	81.41(9), 81.9(2), 81.5(1)
Ru(2)–C(201)	2.404(3), 2.407(7), 2.409(3)	P(1)–C(0)–P(2)	109.6(2), 108.5(3), 109.2(2)
Ru(3)–C(1)	2.433(3), 2.415(7), 2.433(3)	Ru(1)–C(1)–C(2)	89.1(2), 89.0(4), 89.2(2)
Ru(3)–C(2)	2.162(3), 2.149(7), 2.162(3)	Ru(2)–C(2)–C(1)	132.3(2), 133.4(5), 132.5(2)
P(1)–C(0)	1.833(3), 1.839(7), 1.839(4)	Ru(2)–C(201)–C(2)	67.0(1), 66.1(3), 66.5(2)
P(2)–C(0)	1.836(3), 1.837(7), 1.831(4)	C(2)–C(1)–C(101)	129.7(2), 131.1(6), 128.9(3)
C(1)–C(2)	1.355(4), 1.323(9), 1.344(5)	C(1)–C(2)–C(201)	142.1(3), 141.3(5), 142.1(3)
C(1)–C(101)	1.526(4), 1.52(1), 1.534(5)	C(202)–C(201)–C(206)	117.2(3), 117.9(7), 116.4(4)
C(2)–C(201)	1.455(4), 1.48(1), 1.457(5)	C(203)–C(202)–C(201)	121.5(3), 121.1(8), 122.3(5)
C(201)–C(202)	1.415(4), 1.41(1), 1.417(6)	C(204)–C(203)–C(202)	119.8(3), 120.0(9), 119.5(5)
C(201)–C(206)	1.403(4), 1.40(1), 1.392(6)	C(205)–C(204)–C(203)	120.5(3), 119.9(9), 120.5(6)
C(202)–C(203)	1.366(4), 1.35(1), 1.364(8)	C(206)–C(205)–C(204)	120.9(3), 121.1(8), 121.1(5)
C(203)–C(204)	1.388(5), 1.42(1), 1.381(9)	C(201)–C(206)–C(205)	120.0(3), 119.9(8), 120.1(4)
C(204)–C(205)	1.348(5), 1.34(2), 1.333(9)	Ru(2)–H(23)–Ru(3)	111(1), [123(est.)], 117(1)
C(205)–C(206)	1.402(4), 1.39(1), 1.412(7)		
Ru(2)···C(206)	2.557(3), 2.614(8), 2.601(4)		
Ru(2)–H(23)	1.71(2), [1.48(est.)], 1.52(2)		
Ru(3)–H(23)	1.80(2), [1.80(est.)], 1.87(2)		

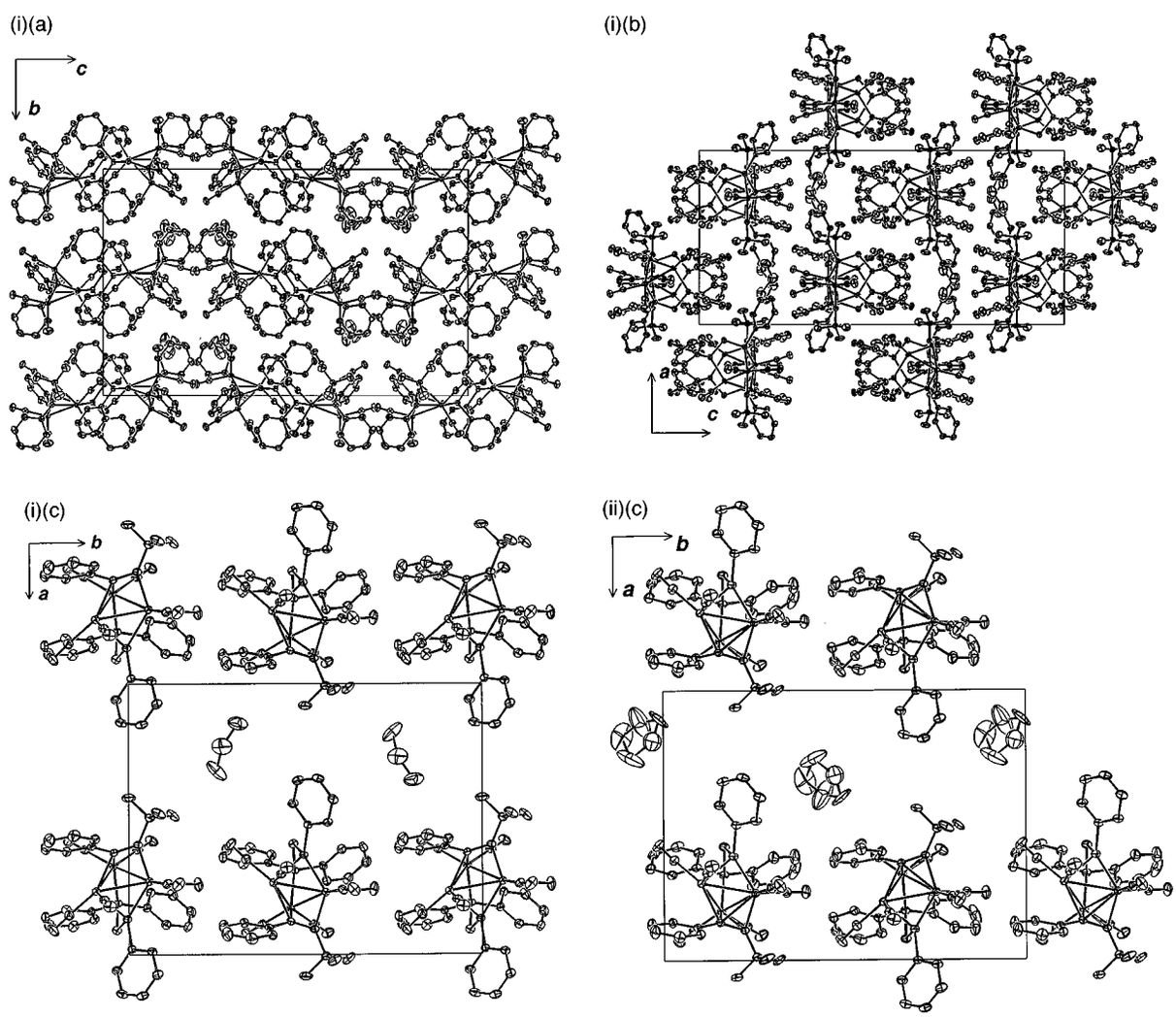

Fig. 2 Unit cell projections down (a) *a*, (b) *b* and (c) *c* (the latter of the layers at $c = 0.13$) of (i) compound **6**. 0.366(3)CH_2Cl_2 and of (ii) **6**·thf [(c) only; views corresponding to (a) and (b) are very similar].

rules and called "basket-like", has been reported for the 48-MVE compound $[Os_3(\mu\text{-}H)_2(\mu_3\text{-}HC_2NEt_2)(CO)_9]$ **9** and related species.[12] Theoretical calculations have demonstrated that the unusual co-ordination of the aminoacetylene ligand to the trimetallic array in **9** is mainly due the π-donor effect of the amino substituent on the alkynyl grouping.[13]

Table 2 Ru_3, phenyl C_6 interplanar dihedral angles (°) (1 thf; 1, 0.366 CH_2Cl_2 solvates, respectively)

Plane	11*n*	21*n*	22*n*	20*n*
Ru_3	48.27(9)	27.0(1)	64.62(9)	45.08(8)
	51.7(2)	31.6(2)	47.2(2)	43.7(2)
	51.5(1)	32.0(1)	46.3(1)	44.1(1)
11*n*		69.6(1)	75.8(1)	82.1(1)
		70.8(3)	87.2(3)	84.4(3)
		70.1(2)	86.8(2)	85.3(2)
21*n*			63.9(1)	53.0(1)
			63.7(3)	60.7(3)
			63.6(2)	61.6(2)
22*n*				22.2(1)
				3.5(3)
				2.2(2)

Deviations of Ru(2) from the C(20*n*) plane are 2.083(3), 2.107(8), 2.112(4) Å. Torsion angles: C(2,1,101,102) −149.9(3), −158.0(8), −156.3(4); Ru(1),P(1),C(111,112) −7.2(3), −4.4(7), −4.5(4)°

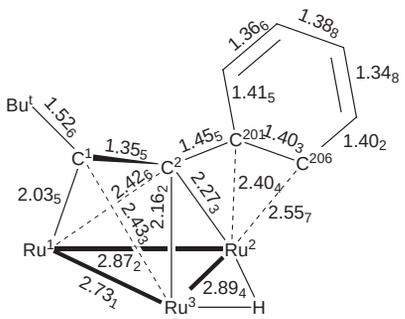

Fig. 3 Detailed geometry of the alkyne–Ru_3 cluster interaction in compound **6**.

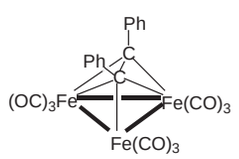

7

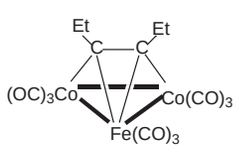

8

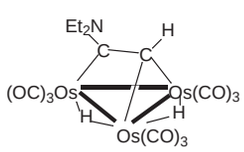

9

With a cluster electron count of 46, compound **6** is unique in featuring an alkyne ligand twisted relative to an M–M bond that is bound with a distorted μ_3-η^2-($\perp$) mode to the cluster framework. Extended Hückel Theory (EHT) and Density Functional Theory (DFT) calculations were carried out on **6** and related models in order to understand why such a distorted geometry for the alkyne ligand is favored in this particular Ru_3 environment (see the Experimental section for details).

DFT Calculations were first performed on the model [Ru_3-(μ-H)(μ_3-$PHCH_2PH_2$)(μ_3-MeC_2Ph)$(CO)_6$] **6′** based on the crystal structure of **6** in order to reduce computational effort. A large HOMO − LUMO gap (2.13 eV) is computed for the count of 46 MVEs. Comparable results were obtained with EHT calculations: the same electron configuration was obtained, with a HOMO − LUMO gap of 1.73 eV. The composition of the MOs in the HOMO − LUMO region is similar for both DFT and EHT results. Therefore, because of its structural complexity (size of the molecule, lack of symmetry) the detailed analysis of the bonding in **6** was carried out using EHT calculations.

The first step was to determine if our results mirror the experimental data. We started by simply rotating the MeC_2Ph ligand relative to a frozen Ru_3(μ-H)(μ_3-$PHCH_2PH_2$)$(CO)_6$ fragment. Indeed, starting from the *closo* arrangement **10**, a slight rotation of *ca*. 20°, bringing C(2) close to Ru(3) and accompanied by the bending of the phenyl group, is sufficient to generate the distorted *closo* (DC) geometry observed in compound **6**. Alternatively, a rotation of the alkyne ligand on the same core bringing C(1) and C(2) close to Ru(3) and Ru(1), respectively, can be envisaged, leading to another DC geometry (**11**), which is not observed experimentally (see Scheme 3).

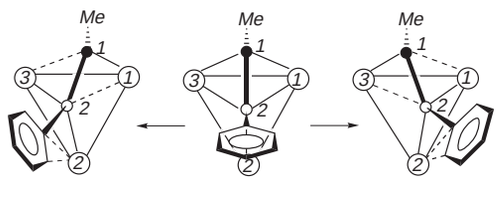

6′ **10** **11**

Scheme 3

Calculations were carried out on the *closo* model **10** with the C(1)–C(2) vector strictly perpendicular to the Ru(1)–Ru(3) bond and compared to those obtained for **6′** and **11**. The alkyne ligand was placed on the top of the Ru_3 triangle similarly to that encountered in the related *closo* cluster [Ru_3(μ_3-PhC_2Ph)-(μ-dppm)$(CO)_7$] **12**.[14] According to EHT calculations the *closo* structure **10** is less stable than the DC structure **6′** by 1.24 eV. The computed bonding energies between the MeC_2Ph ligand and the [Ru_3(μ-H)(μ_3-$PHCH_2PH_2$)$(CO)_6$] fragment are *ca*. 3.0 and 4.0 eV for **10** and **6′**, respectively. Although optimization of the *closo* geometry would somewhat lower its energy, we think nevertheless that the DC arrangement **6′** will have a still lower energy.

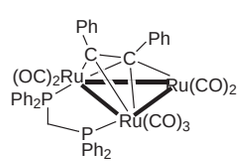

12

The EHMO diagrams for the *closo* **10** and DC **6′** arrangements are compared in Fig. 4. They were built up from the interaction of the frontier molecular orbitals (FMOs) of the metallic Ru_3(μ-H)(μ_3-$PHCH_2PH_2$)$(CO)_6$ fragment with the frontier orbitals of the MeC_2Ph ligand. The metallic fragment exhibits a set of two-below-three FMOs characteristic of triangular M_3L_9 units with an edge bridged by a hydride ligand.[15] The FMO (2a) extends mainly in the Ru_3 plane, whereas the four others (1a, 3a, 4a, and 5a) extend predominantly above the metal plane (see the middle of Fig. 4).

The linear C_2H_2 ligand has two π and two π^* orbitals. Upon co-ordination to a metal framework the H atoms bend back and these two sets lose their degeneracy. Mixing with σ orbitals, one π component (σ/π) is destabilized, while one π^* component (σ/π^*) is stabilized. Replacement of the H substituents by Me and Ph groups modifies the shape and the energy of these FMOs. The C–C bonding π and σ/π FMOs are predominantly localized on C(1) attached to the Me group, and the C–C antibonding π^* and σ/π^* FMOs are slightly more localized on C(2) to which is tethered the Ph group.

In the *closo* structure the main bonding interactions between the two fragments occur between the metallic 3a and 4a FMOs and the alkyne σ/π and π FMOs, respectively, and between the metallic 2a FMO and the σ/π^* and π^* FMOs of the MeC_2Ph ligand. The metallic 1a FMO hardly interacts with the alkyne ligand and remains almost unperturbed after interaction. The

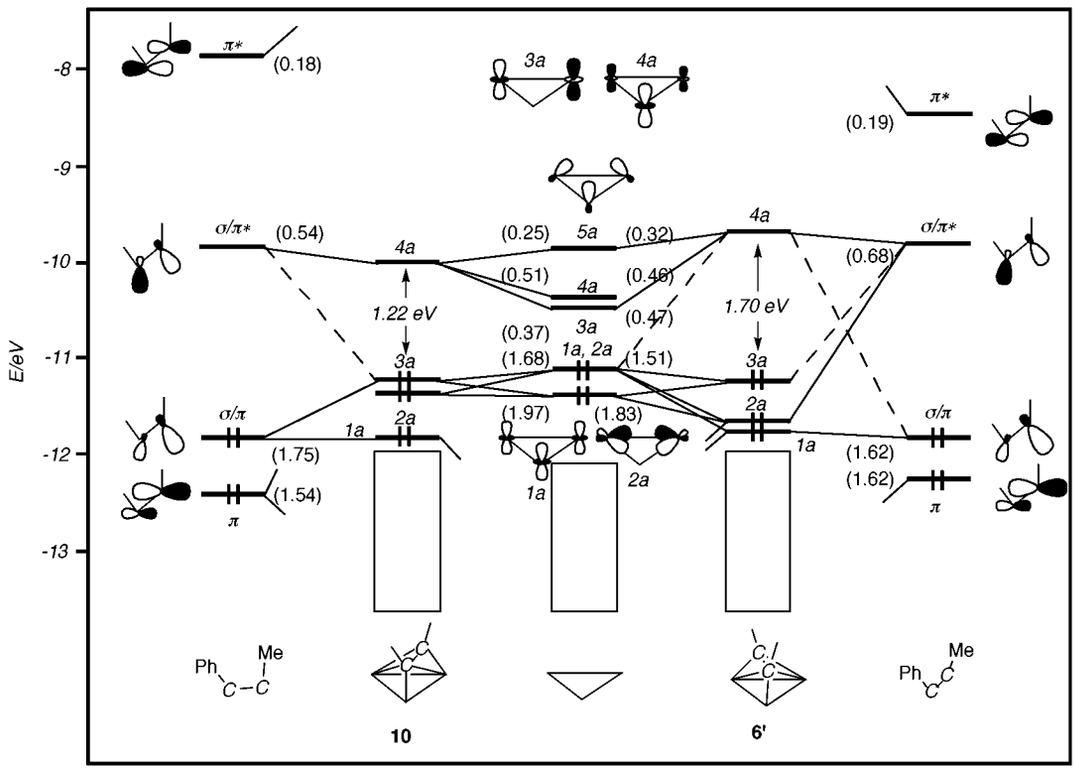

Fig. 4 EHMO Interaction diagram of the model $[Ru_3(\mu\text{-}H)(\mu_3\text{-}PHCH_2PH_2)(\mu_3\text{-}MeC_2Ph)(CO)_6]$ in the *closo* arrangement **10** (on the left) and the DC arrangement **6′** (on the right). FMO occupations after interaction are given in parentheses.

resulting MO diagram of **10** is shown on the left-hand side of Fig. 4. The MO diagram of the DC structure **6′** shown on the right-hand side resembles quite strongly that of the *closo* structure **10** except in the LUMO region. Indeed, the 4a LUMO is pushed up in energy in the DC arrangement and the HOMO − LUMO gap rises to 1.70 eV for the count of 46 MVEs (it is 1.22 eV in the *closo* structure). Such a large HOMO − LUMO gap ensures the stability of this DC arrangement.

Examination of the LUMO reveals a quite strong antibonding character between Ru(2) and carbons of the Ph group tethered to C(2), particularly C(206). Upon bending of the Ph group towards Ru(2), interaction between the metallic fragment and the alkyne ligand increases, in particular between the metallic 2a FMO and the alkyne σ/π* FMO, due to a better overlap, leading to some stabilization of occupied MOs and destabilization of vacant MOs in particular the LUMO. A second-order Jahn–Teller distortion is suspected in the *closo* structure **10**, leading to the more stable DC structure **6′**. The destabilization of the LUMO is accompanied by the stabilization of occupied orbitals (because of the lack of symmetry, we were not able to identify which particular orbitals are stabilized).

We tried to quantify the gain of energy due to the bending of the phenyl ring towards Ru(2) in structure **6′**. A DC arrangement with the Ph group pointing away from Ru(2) is less stable by 1.05 eV and the HOMO − LUMO gap decreases from 1.70 to 1.22 eV, comparable to that computed for the *closo* arrangement **10**. The bonding energy between the two fragments drops from *ca*. 4.0 to 3.2 eV. Clearly the bending of the phenyl group of the alkyne ligand towards Ru(2) with C(1) and C(2) close to Ru(1) and Ru(3), respectively, is essential in stabilizing structure **6′**. Nevertheless, a close look at the atomic net charges indicates almost no change in the electron transfer between the alkyne ligand and the metal framework upon bending of the phenyl ring.

The metallic fragment is very slightly negatively charged before and after bending (−0.21 *vs.* −0.18), indicating that in both cases donation from the alkyne ligand to the cluster is slightly more important than back donation from the cluster to the C_2 ligand. The EH atomic net charges of the metal atoms are −0.49, −0.01 and −0.32 for Ru(1), Ru(2) and Ru(3), respectively. The corresponding charges before approach of C(201) and C(206) were −0.47, −0.17 and −0.28, respectively. Thus, the less electron-rich Ru(2) centre loses some electron density upon bending of the phenyl ring. The charge on atom C(1) of the alkyne, nearly neutral before (+0.02), becomes slightly negative (−0.06) after bending of the phenyl ring, whereas the charge on C(2) remains almost unchanged (−0.04 *vs.* −0.05). The total charge on the phenyl ring becomes slightly more positive after bending (+0.09 *vs.* +0.06 before). We conclude that upon bending of the phenyl ring there is a very weak additional electron transfer from the phenyl ring towards the metal fragment, which in turn transfers some electron density to atom C(1) of the alkyne ligand.

Clearly, the "side on" Ru(2)–C(201, 206) interaction occurring in compound **6** should be regarded as a covalent interaction between metallic orbitals and alkyne FMOs containing some admixture of phenyl carbon atoms. The delocalization of the latter FMOs on the phenyl ring allows the Ru(2) center to establish bonding interactions with C(201) and C(206). The EH overlap populations (OPs) computed between Ru(2) and C(201) and C(206) (0.05 and 0.06, respectively) suggest a non-negligible metal–carbon bonding interaction. For comparison the OP corresponding to the Ru(2)–C(2) bond is 0.22. This is supported by the DFT electron density distribution in the Ru(2)–C(201)–C(206) plane illustrated in Fig. 5. Some electron density is present between Ru(2) and the two close carbon atoms of the phenyl ring.

It is interesting that the alternative DC structure **11** with C(1) and C(2) close to Ru(3) and Ru(1), respectively, and the Ph group bent towards Ru(2) (see Scheme 3) is computed to be 2.01 eV less stable than structure **6′**, with a bonding energy between the alkyne ligand and the metallic fragment of only 2.21 eV. The different ligand environment around the Ru atoms in the $Ru_3(\mu\text{-}H)(\mu_3\text{-}PHCH_2PH_2)(CO)_6$ fragment (see above) renders them electronically non-equivalent. This indicates that the slight twist of the alkyne ligand accompanied by the bending of

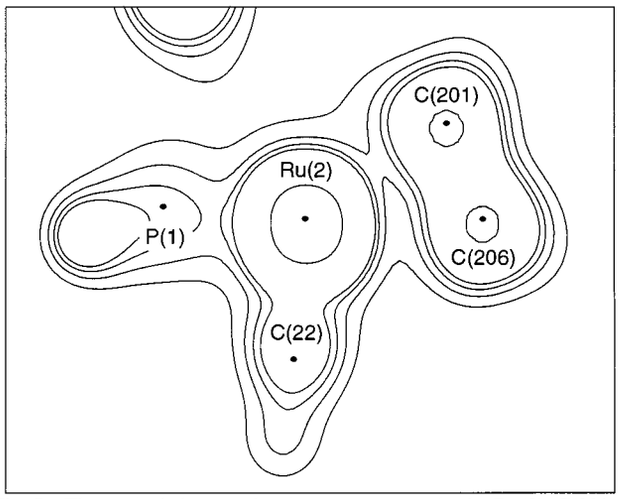

Fig. 5 Theoretical electron density contour map in the Ru(2)–C(201)–C(206) plane of structure **6′**. Atoms P(1) and C(22) are 0.81 and 0.58 Å above the plane, respectively. Contour values are 0.03, 0.05, 0.07, 0.09, and 1.00 e bohr^{-3} (bohr ≈ 5.29 × 10^{-11} m).

the Ph group in **6** is mainly dictated by the stereoelectronic asymmetry of the metallic fragment. Note that a regular *closo* arrangement is observed in $[Ru_3(\mu_3\text{-}PhC_2Ph)(\mu\text{-}dppm)(CO)_7]$ **12** even though it contains a related C_2Ph_2 ligand bound to a symmetrical metal fragment.[14]

In summary, the asymmetry of the metallic fragment in compound **6** obliges the alkyne to rotate with respect to the Ru(1)–Ru(2) vector, somewhat weakening the M–C bonding. This is reflected in the C–C overlap population which is slightly stronger in **6′** than in **10**, indicating that the C_2 unit is less strongly bound to the metal triangle in the former. This M–C bonding weakening is compensated by the approach of two carbon atoms of the Ph group towards Ru(2), somewhat resembling an "agostic" interaction.[16] Comparable "side-on" M–C interactions involving a double bond of the phenyl ring have been previously encountered in electron-deficient metal complexes such as $[Fe_2(\mu\text{-}C_3Ph_3H)(CO)_6]$,[17] $[Fe_2\{\mu\text{-}C(OEt)CPhCHPh\}(CO)_6]$[18] or $[Fe_2(\mu\text{-}CHCHCMePh)(CO)_6]$.[19] Analogously to these complexes, this interaction in **6** induces a partial localization of the C–C bonds of the phenyl ring, which become alternatively short and long (see Table 1). Such a "side-on" M–C interaction is different from those involving co-ordination between a metal center and a C–C (Ph) bond, as found in $[Ru_3\{\mu_3\text{-}CHCPhC(O)CPhCPh\}(\mu\text{-}dppm)(CO)_6]$[14] or a P–C (Ph) bond, as found in $[Ru_3(\mu\text{-}H)(\mu\text{-}PPh_2)(CO)_9]$.[20]

Discussion

The major point of interest in the chemistry reported here is the unusual attachment of the alkyne ligand in complex **6**. Perhaps the closest analogy is to be found in the recently described $[Ru_3\{\mu_3\text{-}CHCPhC(O)CPhCPh\}(\mu\text{-}dppm)(CO)_6]$, obtained from the reaction of phenylethyne with the 46e complex $[Ru_3\{\mu_3\text{-}(\perp)\text{-}C_2Ph_2\}(\mu\text{-}dppm)(CO)_7]$.[14] The former complex is also co-ordinatively unsaturated, the side-on bonding of the C–C (Ph) bond apparently compensating for the loss of a CO group during its formation. The long-known phosphide derivative $[Ru_3(\mu\text{-}H)(\mu\text{-}PPh_2)(CO)_7]$, with a similar P–C (Ph) interaction with a cluster Ru atom is another example of these 'agostic' phenyl groups.[20]

Complex **6** has been formed by migration of a *P*-bonded phenyl group to the σ-bonded carbon of the μ_3-C_2Bu^t ligand in the precursor **5** (R = Bu^t). This may occur by prior migration of the Ph group to the cluster with displacement of CO, followed by further migration to the σ-bonded carbon of the μ_3-acetylide ligand. The actual molecular structure of **6** can be envisaged as an intermediate stage in the transfer of the Ph group from the dppm ligand to the acetylide *via* the cluster; alternatively, it could be considered to illustrate the activation of the stable alkyne towards C–C bond cleavage. In larger clusters, however, the migration of Ph from diphenylphosphinoacetylide ligands has also been observed, the net result being the elimination of PPh groups to the cluster.[21] The unusual co-ordination of the alkyne fragment is found to be a rather distorted $\mu_3(\perp)$ mode.

Conclusion

Pyrolysis of compound **2** has resulted in phenyl transfer from co-ordinated dppm to the μ_3-acetylide ligand to give the alkyne PhC≡CBu^t which, in **6**, is co-ordinated with an intermediate geometry, with the Ph group involved in a side-on 'agostic' bonding. The growing number of examples of this type of bonding suggests that it represents an intermediate or transition state in the overall phenyl transfer or rearrangement reactions.

Experimental

Instrumentation

IR: Perkin-Elmer 1700X FT IR. NMR: Bruker CXP300 or ACP300 (^{1}H at 300.13 MHz, ^{13}C at 75.47 MHz). FAB MS: VG ZAB 2HF (using 3-nitrobenzyl alcohol as matrix, exciting gas Ar, FAB gun voltage 7.5 kV, current 1 mA, accelerating potential 7 kV).

General reaction conditions

Reactions were carried out under an atmosphere of nitrogen, but no special precautions were taken to exclude oxygen during work-up.

Starting materials

Complexes **1**[22] and **5** (R = Bu^t)[7] were prepared as previously described.

Preparation of $[Ru_3(\mu\text{-}H)_2(\mu_3\text{-}PPhCH_2PPh_2)(\mu_3\text{-}PhC_2Bu^t)(CO)_6]$ 6

A solution of $[Ru_3(\mu\text{-}H)(\mu_3\text{-}C_2Bu^t)(\mu\text{-}dppm)(CO)_7]$ (200 mg, 0.207 mmol) was heated in refluxing toluene (50 ml) for 60 h. Evaporation and separation of the products by preparative TLC (acetone–light petroleum, b.p. range 60–80 °C, 3 : 7) gave the major product as an orange band (R_f 0.69). Crystallisation (CH_2Cl_2–MeOH) gave red crystals of $[Ru_3(\mu\text{-}H)(\mu_3\text{-}PPhCH_2PPh_2)(\mu_3\text{-}PhC_2Bu^t)(CO)_6]$ **6** (80 mg, 41%), mp >150 °C (decomp.). [Found: C, 47.08; H, 3.54%; *M* (mass spectrometry) 939; $C_{37}H_{33}O_6P_2Ru_3$ requires C, 47.39; H, 3.44%; *M* 939]. IR: ν(CO) (cyclohexane) 2034m, 2024vw, 2008vs, 1992m, 1977vs, 1954m (br), 1942 (sh) and 1921m cm^{-1}. ^{1}H NMR: δ($CDCl_3$) −17.56 [2 × m (7 peaks), 1 H, Ru–H], 4.06–4.53 (m, 2 H, CH_2), 5.69 (d, J_{PH} = 7 Hz, 1 H) and 7.16–7.77 (m, 19H, Ph). FAB MS (*m*/*z*, relative intensity): 939, M$^+$, 16; 910, [M − H − CO]$^+$, 10; 882, [M − H − 2CO]$^+$, 10; 854, [M − H − 3CO]$^+$, 50; 826, [M − H − 4CO]$^+$, 75; 798, [M − H − 5CO]$^+$, 42; 781, [M − PhC_2Bu]$^+$, 20; 770, [M − H − 6CO]$^+$, 62; 750, [M − 4CO − Ph]$^+$, 25; 691, [Unknown], 40; 634, [M − $PPhCH_2PPh_2$]$^+$, 35; 611, [M − 2H − 6CO − PhC_2Bu]$^+$, 65; 531, [M − C_2Ph − $PPhCH_2PPh_2$]$^+$, 100.

Structure determination of compound 6

The execution of this exercise has occurred over a period of ten years. Initial structure determination studies were undertaken using unique room-temperature single counter/four-circle diffractometer data sets (2θ–θ scan mode; monochromatic Mo-Kα radiation, $\lambda = 0.7107_3$ Å, $T \approx 295$ K) yielding *N* reflections, N_o with $I > 3\sigma(I)$ being considered 'observed' and used in the full matrix least squares refinement after gaussian absorption correction. Anisotropic thermal parameters were refined for the

non-hydrogen atoms, $(x, y, z, U_{iso})_H$ for the ligand and solvent hydrogen atom parameters being constrained at estimated values. Conventional residuals R, R' at convergence are quoted, statistical weights being derivative of $\sigma^2(I) = \sigma^2(I_{diff}) + 0.0004\sigma^4(I_{diff})$.

The initial study was undertaken on an inferior specimen of the thf monosolvate of compound **6** and did not yield a definitive location for the core hydrogen atom component. In an effort to resolve the latter, material recrystallized from dichloromethane was studied; the structure is disposed quasi-isomorphously to the thf solvate in a unit cell of similar symmetry and dimensions, but with a general displacement of y coordinates by *ca*. 1/4 and the cell volume diminished by *ca*. 10%. Difference map residues were modelled in terms of one molecule of solvation (CH_2Cl_2), with the site occupancy set at unity after trial refinement. This determination, although of more useful precision, again did not yield a definitive core hydrogen atom description.

A more suitable specimen of the thf solvate obtained from fresh material yielded extensive data measured to $2\theta_{max} = 70°$, the site occupancy of the solvent refining to unity and a core hydrogen atom being located. At this stage the novelty of the compound was apparent, as was the desirability of some attempt at theoretical modelling of the associated bonding. After this had been carried out, a new generation of equipment was available in the form of a Bruker AXS CCD detector instrument; the latter thf solvate sample was still available, seemingly having preserved its integrity, and it was decided to reexamine the material in this manner to improve, if possible, parameters for incorporation in/comparison with the theoretical model. This was done, the site occupancy of the solvent thf being set at unity after trial refinement and *all* hydrogen atoms other than those of the solvent (which were set constrained with estimated values) being refined in (x, y, z, U_{iso}), with the core hydrogen atom complement as shown. The proximity of the phenyl ring defined by C(20*n*) to Ru(2) was of interest and, given the somewhat different nature of the structure of the dichloromethane solvate, it was decided to revisit that also in case the rather difference lattice packing impacted at all significantly on molecular conformation. It was found that that material also had substantially retained its integrity, yielding useful data; however, refinement of the solvate site occupancy showed that over the years that had diminished to 0.366(3). Again, all hydrogen atoms other than the solvent were refinable in (x, y, z, U_{iso}), with a similar core hydrogen component. Accordingly, we present, hereunder, details for the following determinations (a)–(c): (a) the CCD instrument study of the thf solvate; (b) the single counter instrument study of the CH_2Cl_2 solvate, site occupancy 1; (c) the CCD instrument study of the CH_2Cl_2 solvate, site occupancy 0.366(3).

For the CCD data, full spheres were measured by ω scans (0.3°, 15 s frames) to $2\theta_{max}$ 58° in a $T = 299$ K ambience [N_{tot} data merging to N (unique), R_{int} as cited], data being processed with the proprietary software SAINT and SADABS the latter encompassing an 'empirical absorption correction'. Structure solutions and refinements were carried out using the XTAL 3.4 program system.[23]

Crystal/refinement data for $[Ru_3(\mu\text{-}H)(\mu_3\text{-}PPhCH_2PPh_2)(\mu_3\text{-}PhC_2Bu^t)(CO)_6] \equiv C_{37}H_{32}O_6P_2Ru_3$. Orthorhombic, space group *Pbca* (D_{2h}^{15}, No. 61), $Z = 8$.

(*a*) **6**·thf $\equiv C_{41}H_{40}O_7P_2Ru_3$, $M = 1009.9$, $a = 14.1102(7)$, $b = 19.006(1)$, $c = 32.422(2)$ Å, $V = 8695$ Å^3, $D_c = 1.54_3$ g cm^{-3}; $F(000) = 4032$, $\mu_{Mo} = 11.5$ cm^{-1}, specimen $0.39 \times 0.35 \times 0.23$ mm, '$T_{min,max}$' = 0.73, 0.90, $N_{tot} = 94246$, $N = 11204$ ($R_{int} = 0.032$), $N_o = 9410$, $R = 0.039$, $R' = 0.025$ (statistical weights), $\Delta\rho_{min,max} = -0.55$, 0.74 e Å^{-3}. (The volume of the unit cell in the more precise of the single counter instrument studies was 8667 Å^3; the change may be consequent upon the slightly different temperature, or crystal 'aging'.)

(*b*) **6**·$CH_2Cl_2 \equiv C_{38}H_{34}Cl_2O_6P_2Ru_3$, $M = 1022.7$, $a = 14.218(8)$, $b = 18.512(15)$, $c = 30.105(13)$ Å, $V = 7924$ Å^3, $D_c = 1.71_4$ g cm^{-3}, $F(000) = 4048$, $\mu_{Mo} = 12.5$ cm^{-1}, specimen $0.12 \times 0.12 \times 0.40$ mm, $T_{min,max} = 0.85$, 0.87, $2\theta_{max} = 55°$, $N = 9093$, $N_o = 5089$, $R = 0.043$, $R' = 0.041$ (statistical weights), $\Delta\rho_{min,max} = 0.86$, 1.21 e Å^{-3}.

(*c*) **6**·0.366(3)$CH_2Cl_2 \equiv C_{37}H_{32}O_6P_2Ru_3$. ≈0.366$CH_2Cl_2$, $M = 969.2$, $a = 14.146(3)$, $b = 18.476(3)$, $c = 29.908(6)$ Å, $V = 7816$ Å^3, $D_c = 1.64_7$ g cm^{-3}, $F(000) \approx 3836.3$, $\mu_{Mo} = 13.2$ cm^{-1}, specimen $0.35 \times 0.13 \times 0.12$ mm, '$T_{min,max}$' = 0.69, 0.85, $N_{tot} = 86234$, $N = 10114$ ($R_{int} = 0.026$), $N_o = 7030$, $R = 0.039$, $R' = 0.022$, $\Delta\rho_{min,max} = -0.57$, 0.98 e Å^{-3}. (The diminished cell volume *cf*. **6**·CH_2Cl_2 is consistent with the diminution of solvent site occupancy.)

CCDC reference number 186/1257.

See http://www.rsc.org/suppdata/dt/1999/479/ for crystallographic files in .cif format.

Theoretical calculations

Density functional calculations were carried out on model **6**′ using the Amsterdam Density Functional (ADF) program[24] developed by Baerends and co-workers[25] using non-local exchange and correlation corrections.[26] The atom electronic configurations were described by a double-ζ Slater-type orbital (STO) basis set for H 1s, C 2s and 2p, O 2s and 2p, P 3s and 3p. A triple-ζ STO basis set was used for Ru 4d and 5s, augmented with a single-ζ 5p polarization function. A frozen-core approximation was used to treat the core electrons of C, O, P, and Ru.

Extended Hückel calculations were carried out within the extended Hückel formalism[27] using the program CACAO.[28] The exponents (ζ) and the valence shell ionization potentials (H_{ii} in eV) were respectively: 1.3, −13.6 for H 1s; 1.625, −21.4 for C 2s; 1.625, −11.4 for C 2p; 2.275, −32.4 for O 2s; 2.275, −14.8 for O 2p; 1.6, −18.6 for P 3s; 1.6, −14.0 for P 3p; 2.078, −8.6 for Ru 5s; 2.043, −5.1 for Ru 5p. The H_{ii} value for Ru 4d was at −12.2. A linear combination of two Slater-type orbitals with exponents $\zeta_1 = 5.378$ and $\zeta_2 = 2.303$ with the weighting coefficients $c_1 = 0.5340$ and $c_2 = 0.6365$ was used to represent the Ru 4d atomic orbitals. The different molecular models used were based on the experimental structure **6**.

Acknowledgements

We thank the Australian Research Council for financial support and Johnson Matthey plc for a generous loan of $RuCl_3 \cdot nH_2O$. P. A. H. acknowledges receipt of a University of Adelaide Post-graduate Research Scholarship. J.-F. H. thanks the University of Adelaide and the Centre National de la Recherche Scientifique for his stay at Adelaide in August 1997. K. C. and J.-F. H. thank the Centre de Ressources Informatiques (CRI) of Rennes and the Institut de Développement et de Ressources en Informatique Scientifique (IDRIS-CNRS) of Orsay (project 970649) for computing facilities. Professor J.-Y. Saillard (Rennes) is thanked for helpful discussions.

References

1 A. J. Deeming, in *Comprehensive Organometallic Chemistry*, eds. E. W. Abel, F. G. A. Stone and G. Wilkinson, Elsevier, Oxford, 2nd edn., 1995, vol. 7, ch. 12, p. 683.
2 N. Lugan, J.-J. Bonnet and J. A. Ibers, *J. Am. Chem. Soc.*, 1985, **107**, 4484.
3 M. I. Bruce, E. Horn, O. bin Shawkataly, M. R. Snow, E. R. T. Tiekink and M. L. Williams, *J. Organomet. Chem.*, 1986, **316**, 187.
4 See, for example: M. I. Bruce, G. Shaw and F. G. A. Stone, *J. Chem. Soc.*, *Dalton Trans.*, 1982, 2094; A. J. Deeming, S. E. Kabir, N. I. Powell, P. A. Bates and M. B. Hursthouse, *J. Chem. Soc.*, *Dalton Trans.*, 1987, 1529.
5 M. I. Bruce, P. A. Humphrey, B. W. Skelton and A. H. White, *J. Organomet. Chem.*, 1996, **526**, 85.

6 M. I. Bruce, P. A. Humphrey, B. W. Skelton and A. H. White, *J. Organomet. Chem.*, 1997, **539**, 141.
7 M. I. Bruce, P. A. Humphrey, E. Horn, B. W. Skelton, E. R. T. Tiekink and A. H. White, *J. Organomet. Chem.*, 1992, **429**, 207.
8 M. G. Thomas, E. L. Muetterties, R. O. Day and V. W. Day, *J. Am. Chem. Soc.*, 1976, **98**, 4645.
9 See, for example: M. J. McGlinchey, in *Topics in Physical Organometallic Chemistry*, ed. M. Gielen, Freund Publishing House, London, 1992, vol. 4, p. 41; J.-F. Halet, *Coord. Chem. Rev.*, 1995, **143**, 637 and refs. therein.
10 J. F. Blount, L. F. Dahl, C. Hoogzand and W. Hübel, *J. Am. Chem. Soc.*, 1966, **88**, 292; A. J. Carty, N. J. Taylor and E. Sappa, *Organometallics*, 1988, **7**, 405; D. Osella, L. Pospisil and J. Fiedler, *Organometallics*, 1993, **12**, 3140.
11 S. Aime, L. Milone, D. Osella, A. Tiripicchio and A. M. Manotti Lanfredi, *Inorg. Chem.*, 1982, **21**, 501.
12 R. D. Adams and J. T. Tanner, *Organometallics*, 1988, **7**, 2241; A. J. Deeming, S. E. Kabir, D. Nuel and N. I. Powell, *Organometallics*, 1989, **8**, 717.
13 Z. Nomikou, J.-F. Halet, R. Hoffmann, J. T. Tanner and R. D. Adams, *Organometallics*, 1990, **9**, 588.
14 S. Rivomanana, C. Mongin and G. Lavigne, *Organometallics*, 1996, **15**, 1195.
15 B. E. R. Schilling and R. Hoffmann, *J. Am. Chem. Soc.*, 1979, **101**, 3456; J.-F. Halet, J.-Y. Saillard, R. Lissillour, M. J. McGlinchey and G. Jaouen, *Inorg. Chem.*, 1985, **24**, 218.
16 M. Brookart and M. L. H. Green, *J. Organomet. Chem.*, 1983, **250**, 395.
17 G. Gervasio and E. Sappa, *Organometallics*, 1993, **12**, 1458.
18 I. Ross, R. Mathieu, X. Solans and M. Font-Altaba, *J. Organomet. Chem.*, 1984, **260**, 240.
19 G. Dettlaf, U. Behrens and E. Weiss, *Chem. Ber.*, 1979, **110**, 3019.
20 S. A. MacLaughlin, A. J. Carty and N. J. Taylor, *Can. J. Chem.*, 1982, **60**, 87.
21 M. I. Bruce, B. W. Skelton and A. H. White, *J. Organomet. Chem.*, 1991, **420**, 87.
22 M. I. Bruce, B. K. Nicholson and O. bin Shawkataly, *Inorg. Synth.*, 1989, **26**, 325.
23 S. R. Hall, G. S. D. King and J. M. Stewart (Editors), *XTAL Reference Manual, Version 3.4*, University of Western Australia, Lamb Press: Perth (1995).
24 Amsterdam Density Functional (ADF) Program, release 2.0.1, Vrije Universteit, Amsterdam, 1996.
25 E. J. Baerends, D. E. Ellis and P. Ros, *Chem. Phys.*, 1973, **2**, 41; E. J. Baerends and P. Ros, *Int. J. Quantum. Chem.*, 1978, **S12**, 169; P. M. Boerrigter, G. te Velde and E. J. Baerends, *Int. J. Quantum Chem.*, 1988, **33**, 87; G. te Velde and E. J. Baerends, *J. Comput. Phys.*, 1992, **99**, 84.
26 A. D. Becke, *Phys. Rev A.*, 1988, **38**, 3098; J. P. Perdew, *Phys. Rev B.*, 1986, **33**, 8822; **B34**, 7406 (erratum).
27 R. Hoffmann, *J. Chem. Phys.*, 1963, **39**, 1397.
28 C. Mealli and D. Proserpio, *J. Chem. Educ.*, 1990, **67**, 399.

Paper 8/07008C